UC Berkeley
UC Berkeley Previously Published Works

Title

Fracture Evolution in Multimineral Systems: The Role of Mineral Composition, Flow Rate, and Fracture Aperture Heterogeneity

Permalink

https://escholarship.org/uc/item/4v39q4s1

Journal

ACS Earth and Space Chemistry, 2(2)

ISSN

2472-3452

Authors

Deng, Hang
Steefel, Carl
Molins, Sergi
et al.

Publication Date

2018-02-15

DOI

10.1021/acsearthspacechem.7b00130

Peer reviewed

Fracture Evolution in Multimineral Systems: The Role of Mineral Composition, Flow Rate, and Fracture Aperture Heterogeneity

Hang Deng,*,† Carl Steefel,† Sergi Molins,† and Donald DePaolo†,‡

† Lawrence Berkeley National Laboratory, Berkeley, California 94720, United States ‡ Earth and Planetary Science, University of California, Berkeley, Berkeley, California 94720, United States

*E-mail: hangdeng@lbl.gov.

Abstract

Geochemical reactions add complexity to the characterization and prediction of fracture hydraulic properties because they depend on factors that are highly heterogeneous, such as mineral composition. However, systematic analyses of fracture evolution in mineralogically heterogeneous systems are still limited. In this study, we investigated fracture evolution in multimineral systems using a reduced dimension reactive transport model. The model was developed and tested based on experimental studies and addresses the complex morphological and geochemical changes that arise from the presence of multiple minerals of different reactivities. Numerical experiments were performed using randomly generated initial fracture geometries based on representative geostatistics, different categories of mineral composition, and a range of flow rates that are relevant to geologic carbon storage systems. The simulation results showed distinct dissolution regimes at different flow rates, each of which produced characteristic dissolution patterns and temporal evolutions of chemical reactions and fracture hydraulic properties. Overall, as flow rate increases, fracture evolution shifts from compact dissolution to fracture channelization to uniform dissolution. The corresponding flow rate for a given dissolution regime, however, varies considerably with mineral composition. Fracture evolution, especially in the flow regime that induces fracture channelization, is also affected by initial fracture geometry. The numerical experiments were used to develop a multireaction Damköhler number (mDa) for the prediction of fracture evolution, and fracture channelization in particular, in multimineral systems. The multireaction Damköhler number also provides a useful framework for the evaluation of caprock integrity in geologic carbon storage systems.

KEYWORDS: fracture evolution, mineral heterogeneity, reactive transport model, multireaction Damkohler number,¨ geologic carbon storage, caprock integrity

1 Introduction

Fractures, natural and induced by anthropogenic activities, are abundant in various geological systems, including the weathered rock and soil layers and karst aquifers in the Earth's critical zone and deep geological formations that are used for energy recovery and waste disposal.(1-4) Fractures serve as preferential flow pathways in these geological systems, especially in

otherwise impermeable rocks, and thus dominate gas and fluid flow and mass transfer in the geosphere.(5-8) In fractured geological systems where corrosive fluids or non-native chemicals are introduced, such as in the injection of acidic fluids for geologic CO_2 storage and hydraulic fracturing, geochemical reactions (e.g., mineral dissolution and precipitation) are promoted.(9) As a result of these chemical reactions, fracture morphology and hydraulic properties (i.e., fracture hydraulic aperture and intrinsic fracture permeability) are subject to alteration. Quantification of flow and transport in fractured rocks, which is needed for reservoir-scale simulations and for interpreting field observations, may require explicit representation of discrete fractures,(10) making fundamental understanding of the dynamic evolution of individual fractures critical.

Previous studies have shown that flow rate plays an important role in controlling fracture alteration that is driven by mineral dissolution.(11-15) The dissolution patterns show distinct features at different flow regimes. At a flow rate that is slow compared to the reaction rate, i.e., the residence time of the fluid is much longer than the time scale of reactions, local equilibrium is likely to be achieved. In this transport-controlled regime, diffusion may become important, which tends to reduce the local concentration gradient and suppress reactive instability.(15, 16) As a result, reactions and the resulting aperture change are limited to the inlet of the flow. This is also known as compact dissolution or face dissolution. At a flow rate that is fast in comparison to the reaction rate, the residence time of the fluid is short, and local reactions become surface reaction controlled. In this case, highly reactive fluids persist throughout the length of the fracture, and dissolution is uniform in the fracture. At flow rates that are comparable to the reaction rate, the interplay between flow and reactions leads to reactive infiltration instability (a form of geochemical self-organization phenomena), i.e., the perturbations due to geometric, flow, and geochemical heterogeneity are amplified to create preferential flow channels in the fractures.(17)

Hydraulic properties of the fractures evolve according to the dissolution patterns. In the case of compact dissolution, fracture permeability does not increase significantly because of the lack of fracture opening at the downstream end. In the case of uniform dissolution, fracture permeability will increase substantially when no confining stress is present and can decrease under confining stresses because of the removal of asperities, i.e., contact points.(12, 18) Fracture channelization leads to a rapid increase in fracture permeability, even under confining pressure, as asperities in nonchannelized regions in the fracture are preserved and can prevent the fracture from closing.(18) The dimensionless Damköhler number, which is defined as the ratio between the reaction and flow rates, has been widely used to analyze dissolution patterns in fractures and porous media under different flow regimes.(11, 13, 15, 19) The interplay between flow and reaction and the resulting dissolution patterns are scale dependent. The use of the Damköhler number provides a unified framework to analyze the evolution of fractures of

different length and mineral dissolution rate. These analyses, however, focused on simple geochemical systems, where typically only a single mineral is present, as the choice of a single reaction rate in multimineral systems is less clear.(20, 21)

As revealed by several experimental studies, however, heterogeneity in mineral composition can cause complex alteration of fracture morphology and hydraulic properties.(22-31) When mineral grains of different reactivities are mixed, preferential dissolution of the fast-reacting mineral(s) leaves behind a porous layer that is composed of the remaining slow-/nonreacting minerals. This altered layer serves as a barrier that limits the contact between the fresh reactive fluid and the fast-reacting mineral, resulting in increasingly reduced dissolution of the fast-reacting mineral.(25, 31) A similar phenomenon has been observed in the Earth's critical zone, where weathering rinds coat unweathered cores of rocks.(32) In fractures, the presence of the altered layer can limit the increase of fracture aperture and fracture permeability.(22, 25, 33) In certain cases where the altered layer has a large porosity and is structurally weakened, the altered layer can detach from the fracture surface or erode. If there is fracture wall erosion, the mobilized particles are transported downstream by the fluid, where they can accumulate at narrow points and reduce fracture hydraulic permeability. (23, 30) In cases where a channel forms, the mobilized particles may be transported by the flow without clogging the fracture or leading to fracture permeability decrease.(23, 34)

These experimental studies have provided important insights regarding fracture alteration in multimineral systems, which are more common in the natural environment. For the same multimineral sample, the spatial patterns of fracture aperture change were observed to shift from compact dissolution to wormholing to uniform dissolution as the flow rate increases.(26) Péclet number, a measure of the relative magnitude of diffusion and advection rate, has been used to describe the flow regimes corresponding to different fracture dissolution patterns. It does not, however, include any information on the reaction rate and therefore limits the ability to compare across mineral compositions. It has been shown that the flow regime corresponding to a given spatial pattern can be different for a mineralogically heterogeneous sample from what would be expected if no mineral heterogeneity was present. For example, channelization was not observed in an argillaceous limestone even though flow conditions that favor channelization in a pure limestone fracture were used.(23) In addition, development of the altered layer at a given flow rate was observed to vary with mineral composition.(25) Most experimental studies, however, are performed under a limited range of conditions (e.g., length, flow rate) and include sample heterogeneity that is difficult to characterize and thus do not allow systematic and quantitative analyses of fracture evolution as a function of mineral composition.

The objective of the current study is to develop an analytical framework for the investigation of fracture evolution, and fracture channelization in particular, in multimineral rock matrices such that comparison across mineral compositions is possible. To this end, we first conduct a series of numerical experiments to examine fracture evolution in multimineral systems under different flow conditions and with different levels of geometric and mineralogical heterogeneity. This investigation is enabled by the recent development of a reduced dimension reactive transport model.(34, 35) Alternative 3D models would involve explicit discretization in the dimension of the fracture aperture using either the pore-scale approach where the fracture surface is resolved explicitly or the dual-continuum approach.(36) 3D models, however, are computationally demanding as fine meshing is typically required given the relatively small aperture size and altered layer thickness compared to fracture plane dimensions. In contrast, the reduced dimension model used in our study is computationally efficient. Further, the model can be viewed as conceptually similar to a dual-porosity model where the exchange between the fracture and the matrix is calculated with the rate model (eqs 4–6). The model was developed and tested based on experimental studies and captures the complex morphological and geochemical changes that arise from the coexistence of minerals of differing reactivity. The key features of the model are summarized in the Methods section including flow conditions, initial fracture geometries, and geochemical conditions like mineral composition used for the numerical experiments. In the Results and Discussion section, we present the results of the numerical experiments and a multireaction Damköhler number (mDa) that can be used to predict and compare dissolution regimes of fractures across mineral compositions. The multireaction Damköhler number provides a framework for the generalization of existing experimental studies and numerical simulations. We conclude the manuscript with a discussion of the implications for caprock integrity in geological carbon storage systems.

2 Methods

2.1 Reduced Dimension Reactive Transport Model

To simulate dissolution-driven fracture alteration, we adopt a reduced dimension model that was developed and tested based on experimental observations. Details of the model can be found in previous publications,(34, 35) and only the key features of the model are summarized here.

The reduced dimension model is implemented in CrunchFlow, a multicomponent reactive transport code.(37) The reduced dimension model includes three modules. The core module provides the fundamental framework in which the fracture is discretized into a 2D mesh within the fracture plane. Each grid cell is a continuum, i.e., fracture and rock matrix coexist. The governing advection-diffusion-reaction (eq 1) is discretized using the integrated finite difference method following the 2D mesh and solved for the total concentration of each component (ψ_i). The Darcian flux ($\boldsymbol{u}$) is solved

using Darcy's law and permeability, which is calculated from local fracture aperture ($b_{i,j}$) using the cubic law.[38] The isotropic tensor ($\mathbf{D}$) includes molecular diffusion. The reaction term (R_i) accounts for the contribution from dissolution (negative) and precipitation (positive) reactions of minerals. Porosity of each grid cell is calculated based on local fracture aperture and updated over time.

(1)

Although the configuration of the core module allows the consideration of fracture aperture variations and therefore fracture geometry heterogeneity, the dimension across the fracture aperture is not treated explicitly, i.e., it is not discretized. Two additional modules were developed to account for the processes across the fracture aperture, specifically the development of an altered layer on the fracture surface and its erosion due to the detachment of the altered rock matrix. It is assumed that the two fracture halves are symmetric.

In the altered layer module, the reaction front for each individual mineral is tracked based on its respective reaction rate and volume fraction. As a result of differential dissolution, mineral fronts retreat into the rock matrix at different rates. The aperture of a given mineral ($b_{i,j,mn}$) is the distance between the dissolution fronts of this mineral (m_n) in both sides of the fracture, i.e., the thickness of the region where this mineral is depleted, including the fracture aperture itself, and a portion of the matrix. The mineral-specific aperture is calculated using eq 2 from the volume fraction of that mineral in the intact rock matrix ($f_{r,i,j,mn}$) and the volume fraction of the mineral in the grid ($V_{i,j,mn}$), which is controlled by the reaction rate of the mineral.

(2)

where d_z is the thickness of the simulated domain in the third dimension perpendicular to the fracture plane. The mineral front that retreats the slowest defines the fracture surface, and the distance between the two fracture surfaces is the fracture aperture, also referred to as the flow aperture or geometric aperture in this study ($b_{i,j}$) (eq 3).

$$b_{i,j} = \min\{b_{i,j,m_1}, ..., b_{i,j,m_n}\} \quad (3)$$

The distance between the fracture surface and the mineral front that retreats the fastest is the thickness of the altered layer (L). Following previous observations,[23, 39] only diffusion and no flow is considered in the altered layer. Given that the dissolution products of the fast-reacting mineral have to diffuse through the altered layer, the dissolution of the fast-reacting mineral is increasingly subject to a diffusive transport limitation as the altered layer develops. This diffusion limitation, as quantified by the diffusion controlled

reaction rate (R_{diff}), is proportional to the ratio between the effective diffusion coefficient of the porous altered layer (D_{eff}) and its thickness (eq 4). The effective reaction rate (R_{eff}) (eq 5) is determined by the lower value of R_{diff} and the surface reaction rate R_{surf}, which is calculated using transition state theory type rate laws in this study. In eq 6, k_{rxn} is the kinetic coefficient, A_{rxn} denotes the reactive surface area, IAP represents the ion activity product, and K_{eq} is the equilibrium constant. The exponents n_1 and n_2 here are assumed to be one.

$$R_{diff} \propto \frac{D_{eff}}{L} \quad (4) \qquad R_{eff} = \frac{1}{\frac{1}{R_{diff}} + \frac{1}{R_{surf}}} \quad (5)$$

 (6)

These formulations enable the consideration of the development of the altered layer and the diffusion limitation on subsequent geochemical reactions in the fracture. The dissolution front for each individual mineral and the altered layer thickness are calculated internally and updated dynamically in the model. The only additional input parameter is D_{eff}, which can be calculated from the porosity of the altered layer, i.e., the sum of the porosity of the intact rock matrix and the volume fraction of the fast-reacting mineral, using Archie's law.

The erosion module accounts for the observation that dissolution of a fast-reacting cementing mineral can result in disaggregation and detachment, i.e., erosion, of the altered layer. The erosion rate of the altered layer (E [m/s], eq 7) is formulated as a function of the thickness of the altered layer, which provides a measure of the extent of dissolution of the cementing material. The erosion of the altered layer is triggered after a critical thickness (L_c) is exceeded. This is consistent with the physical process that a mineral grain can only detach from the rock matrix after the bulk of the cementing mineral is removed. The parameters η, L_c, and ε are empirical constants depending on the composition and texture of the altered layer.

 (7)

## 2.2 Initial Fracture Geometries

Initial fracture geometries used in the numerical simulations are random fields generated based on a log-normal distribution and geometric statistics reported for fractures used in previous experimental studies (Table 1).(34, 40, 41) The fracture domain is 5.08 cm long and 2.54 cm in width, which is consistent with the typical sample size used in core-flooding experiments.

Table 1. Average Aperture, Standard Deviation of Apertures, and Spatial Correlation Length Reported in the Literature[34,40,41] and of the Generated Random Fields[a]

	the Indiana limestone	the Duperow dolomite	the Niobrara shale	RF1	RF2	RF3	RF4
average (μm)	187–263	128	39	132(130)	122(130)	40	39(40)
standard deviation (μm)	151–196	71	32	69(70)	65(70)	30	32(30)
correlation length (μm)	1800–4200	1350–2400	4355	1500	4500	1500	4500

[a]For the generated random fields, the values used are reported in parentheses when different from the resulting values.

Two average aperture values, 130 and 40 μm with standard deviations of 70 and 30 μm, respectively, were used to generate the random fields. For each combination of aperture statistics, two correlation lengths, 1500 and 4500 μm, were considered. A grid size of 200 μm was used to generate the random fields (Figure 1), which is also the size of the grid cells used in the simulations. The statistics of the generated random fields are summarized in Table 1. Compared to random fields #3 and #4 (RF3 and RF4), random fields #1 and #2 (RF1 and RF2) have smaller roughness as measured by the ratio between the standard deviation of fracture apertures and the average aperture. RF1 and RF3 are generated with a shorter spatial correlation length.
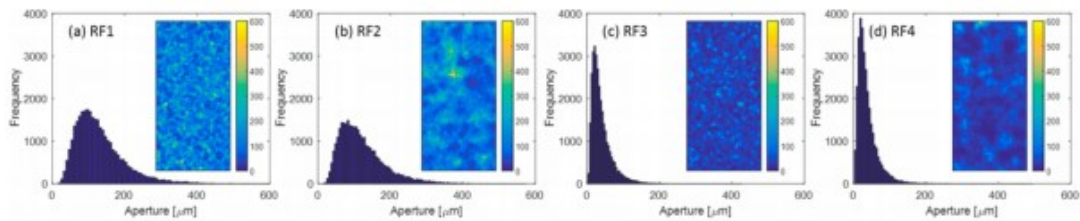
Figure 1. Histograms and maps of the initial fracture apertures [μm] used in the simulations. (a–d) Random fields #1–4 (RF1–RF4).

The fracture aperture values capture the range documented for most types of rocks in the geosphere, except for large fissures that may be present in geothermal or karst environments.(6) Overall, our array of fracture aperture parameters provides an ensemble of possible geometric heterogeneity characteristics and allows us to examine their controls on fracture alteration patterns.

2.3 Mineral Composition

Three types of mineral composition are considered. The first type is composed of a single carbonate. One example is the Indiana Limestone. As there is no heterogeneity in mineral composition, it allows us to establish a baseline for fracture evolution with impacts from only geometric heterogeneity and flow rates. The second type includes two carbonate minerals of differing reactivity with the fast reacting mineral making up a small (<30% by volume) proportion of the rock. The Duperow dolomite, in which ~10% of calcite is dispersed in a dolomite, is representative of this rock type. The third type of mineral composition is a carbonate-rich shale, i.e., the amount of a fast-reacting mineral like calcite is large (>30% by volume) and coexists with clay minerals and other silicates that are relatively

slow reacting. Examples of this type of mineral composition include the Eagle Ford shale and the Niobrara shale.

For type I mineral composition, two cases, pure calcite and pure dolomite, are simulated for comparison with the other two types of mineral composition. For types II and III, the mineral composition follows the Duperow dolomite and the Niobrara shale, respectively (Table 2). This is because the underlying processes involved in fracture alteration in the two rocks and the corresponding parameters were well understood and documented through previous fracture flow experiments.(34, 35)

Table 2. Mineral Volume Fraction [%] and Porosity [%] of the Three Types of Mineral Compositions Used in the Numerical Simulations[a]

	type I: single carbonate		type II: low calcite carbonate					type III: calcite-rich shale		
calcite	85		9[a]	5	20	30	47.9[b]		35	60
other minerals		dolomite 90	dolomite 81	85	70	60	illite 17.0, quartz 14.8, dolomite 6.4, smectite 6.3, plagioclase 3.6, pyrite 1.0		illite 31, quartz 31	illite 18.5, quartz 18.5
porosity	15	10	10	10	10	10	3		3	3

[a]The Duperow dolomite. [b]The Niobrara dolomite.

The specific choice of the Duperow dolomite and the Niobrara shale does not mean that the model cannot be applied to other mineral compositions. Previous studies provide valuable insights as to what processes–mineral dissolution, diffusion-limited reaction due to an altered layer, and erosion of the altered layer–are in play for a given mineral composition. For example, the diffusion limitation from the altered layer can only be present for multimineral systems where the altered layer is able to develop, and the erosion of the altered layer is triggered only when the fast-reacting mineral is also the cementing material and exceeds a certain volume fraction of the rock. The structural strength of the altered layer will be strong enough to maintain a connected framework, and erosion will not occur if the volume fraction of the cementing mineral is too low. A threshold of 35% was suggested based on comparisons between previous experimental studies that observe detachment of the altered layer and those that do not and based on the systematic behavior observed in shales.(34, 42)

In fact, several generalized mineral compositions are used in this study to investigate how variations in calcite content could affect fracture evolution for a given type of mineral composition (section 3.3). For the low calcite carbonate (type II), three additional compositions were considered, where calcite accounts for 5, 20, and 30% of the rock matrix. The amount of dolomite changes accordingly with the porosity of the intact rock matrix fixed at 10%. The effective diffusion coefficient is calculated using the respective altered layer porosity and Archie's law with parameters reported in Deng et al. (2016).(35) For the calcite-rich shale (type III), two additional compositions were considered with calcite contents of 35 and 60%, respectively. For these two calcite-rich shales, the remainder of the rock matrix consists of equal proportions of quartz and illite, and the porosity of the intact rock matrix is 3%. The effective diffusion coefficient for the shale

compositions is calculated using the respective altered layer porosity and parameters that are reported for the Niobrara shale.(34) Coefficients for the erosion rate from Deng et al. (2017)(34) were used. Different coefficients are also explored to examine their impacts on fracture alteration.

All simulations are performed at 25 °C, and the kinetic coefficients used are summarized in Table 3. We note that higher temperatures may be encountered in the subsurface, but we do not expect that using different temperature values will affect the validity of our analyses.

Table 3. Thermodynamic and Kinetic Data of Minerals Present in the Simulations[a]

mineral	log K_{eq}	kinetic coefficients (log k_i) (mol m^{-2} s^{-1})	
calcite[b]	8.2	$k_{rxn} = k_1 a_{H^+} + k_2 a_{H_2CO_3^*} + k_3$	-1.08, -3.96, -4.82
dolomite[b]	15.2	$k_{rxn} = k_1 a_{H^+}^{0.5}$	-3.35
illite[c,e]	9.0	$k_{rxn} = k_1 a_{H^+}^{0.52}$	-11
quartz[c]	-4.0	k_{rxn}	-13.2
smectite[d]	11.0	$k_{rxn} = k_1 a_{H^+}^{0.34} + k_2$	-10.98, -12.78
albite[c,e]	2.8	$k_{rxn} = k_1 a_{H^+}^{0.34}$	-10.07
pyrite[d]	-24.6	$k_{rxn} = k_1 a_{H^+}^{-0.5} a_{Fe^{3+}}^{0.5}$	-7.9

[a]The equilibrium constants (K_{eq}) are from the EQ3/6 database, and the kinetic data are from Palandri and Kharaka (2004),[43] Marty et al. (2015),[44] and Deng et al. (2016)[35]. [b]Deng et al. (2016).[35] [c]Marty et al. (2015).[44] [d]Palandri and Kharaka (2004).[43] [e]Because the reactive fluid used in the experiment is highly acidic, mechanisms for neutral and basic environments are negligible and not included. Only the pH dependence is considered for the kinetic reaction.

For each mineral composition, all four initial fracture geometries are simulated. Even though Table 1 indicates that fractures in carbonate rocks tend to have larger apertures in general, probably because of coarser grain size, there are no definitive correlation between mineral composition and fracture aperture size reported.

2.4 Flow and Other Geochemical Conditions

A constant volumetric flow rate was imposed as the boundary condition. For each combination of geometry and mineral composition, three volumetric flow rates (10, 100, and 1000 μL/min) were simulated. These values are within the range that may be encountered in a natural and engineered subsurface environment. For these flow rates, the Péclet number values are high and indicate that advection is more important than diffusion in the simulations. Although pressure conditions are typically more realistic boundary conditions, we use the constant flow rate here so as to maintain constant nondimensional parameters (especially Damköhler numbers) for the various simulations.

For a given pressure gradient (∇P) and hydraulic aperture (b_h), the flow rate (Q) through a fracture can be calculated from eq 8.

$$\qquad\qquad\qquad (8)$$

where W is the width of the fracture and μ is the dynamic viscosity.

The hydrostatic pressure gradient is on the order of 0.01 MPa/m, and the pressure gradient may reach 1 MPa/m due to fluid injection, e.g., geologic carbon storage and hydraulic fracturing. Assuming a hydraulic aperture within the range of 10–500 μm,(6) the resulting flow rate is 1–10000000 μL/min.

In the simulations, fracture apertures and thus the pressure gradient across the fracture evolve as a result of geochemical reactions. The updated pressure gradient was then used in a rearranged version of eq 8 to calculate the hydraulic aperture to quantify the change of fracture hydraulic properties over time. Fracture hydraulic aperture is related to fracture permeability by a power law relationship and is used in this study as a measure of fracture hydraulic properties because it can be readily compared with geometric fracture aperture. Hydraulic aperture is equal to the average geometric aperture, also referred to as the mechanical aperture, in parallel plate fractures and deviates from the mechanical aperture in the presence of geometric heterogeneity.

Simulations were run for 100 h except for some low flow rate simulations, which were run for 1000 h. The longer simulation time ensures similar pore volumes to the high flow rate simulations and more observable changes in the fractures.

For all simulations, the influent is a CO_2-saturated fluid with a total dissolved carbon concentration of 1.2 mol/L and a pH of 3.2.

3 Results and Discussion

In this section, we will first show the evolution of fracture geometry, geochemical reactions, and fracture hydraulic properties from the simulations that use a single carbonate mineral and discuss the impacts of flow rates and geometric heterogeneity. This discussion is followed by the simulation results of the low calcite carbonate and the calcite-rich shale and discussions of the role of heterogeneity in mineral composition. At the end of this section, time scale analyses in multimineral systems are introduced to provide a general framework for analyzing fracture evolution in such systems.

3.1 Homogenous Mineral Composition

In this subsection, we first focus on the different behaviors in fracture evolution caused by varying flow rate and discuss the observations that are consistent across initial fracture geometries. Then, we discuss the variations in fracture evolution that are due to differences in fracture geometry for a given flow regime.

3.1.1 The Role of Flow Rate

Figure 2 plots the changes in fracture apertures after 100 h of reactive flow at the three flow rates for the four initial fracture geometries for the pure calcite case. At the flow rate of 10 μL/min, calcite dissolution and aperture

increase are limited at the inlet. Instabilities observed at the inlet propagate only a small distance into the fractures. At 100 μL/min, the instabilities are preserved and amplified, leading to the development of evident channels that penetrate deep into the fractures. As the flow rate increases further (at 1000 μL/min), the instabilities are smoothed out, and the dissolution becomes highly uniform. This is because, at the high flow rate, mineral dissolution is surface reaction controlled, and fluid reactivity is maintained throughout the fracture.
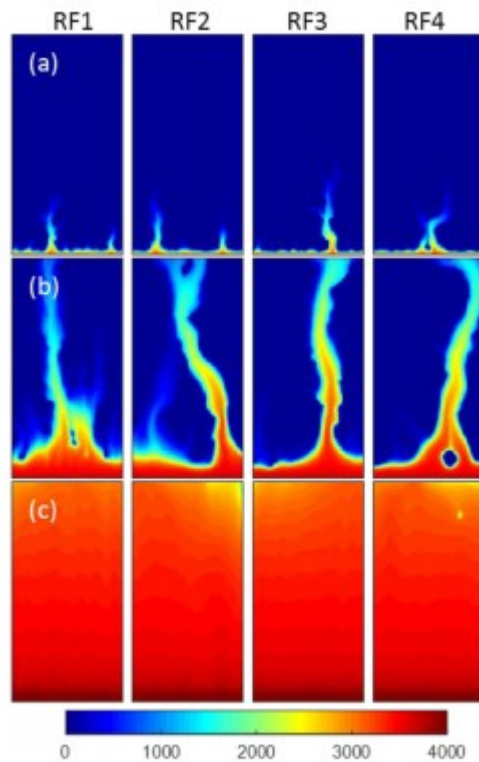
Figure 2. Simulated aperture change [μm] for the pure calcite case after 100 h of reactive flow at a rate of (a) 10, (b) 100, and (c) 1000 μL/min. Each column corresponds to an initial fracture geometry. From left to right: RF1–RF4.

The effluent Ca concentration at a flow rate of 10 μL/min is stabilized at ~40 mM, indicating that the reaction in the fracture has reached equilibrium across all geometries (Figure 3(a)). At 100 μL/min, the concentration decreases from 40 to ~30 mM by the end of the simulation. This is consistent with the observation that effective surface area, and thus overall reaction rate, is reduced due to flow channeling.(28, 40) At 1000 μL/min, the concentration is much lower because the residence time is so short that there is insufficient time for local reaction to approach equilibrium. However, given the large volumetric flow rate, the total amount of dissolution after the same period of flow is highest in this case. As a result, the fracture volume at the highest flow rate is increased by 30–90× across the four fracture geometries (Figure 2(c)). This means that, over time, a smaller fraction of

the fluid that flows through the fracture is in contact with the reactive mineral, leading to a decrease in the effluent Ca concentration (Figure 3(a)).
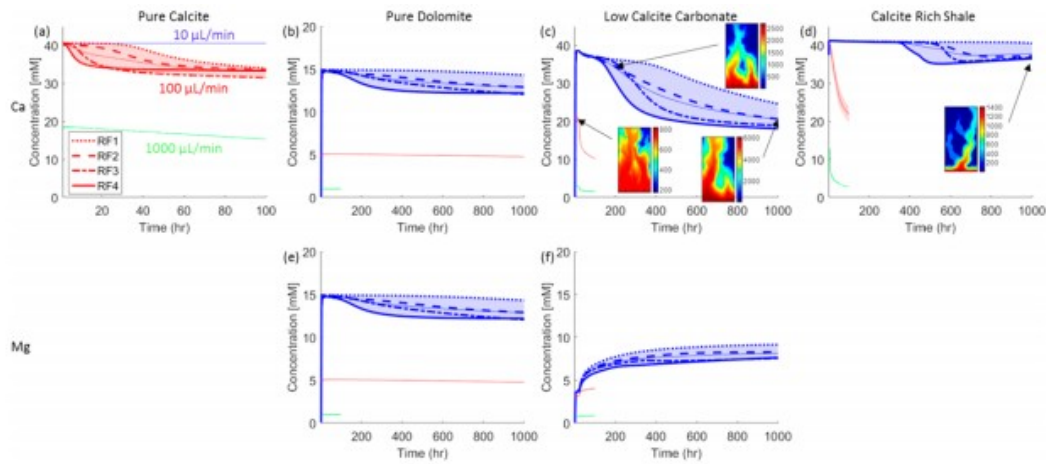
Figure 3. Effluent Ca (a−d) and Mg (e, f) concentrations at 10 (blue), 100 (red), and 1000 (green) μL/min for the mineral composition of pure calcite (a), pure dolomite (b, e), low calcite carbonate (i.e., the Duperow dolomite) (c, f), and calcite-rich shale (i.e., the Niobrara shale) (d). The shaded areas illustrate the variations among different initial fracture geometries with the thin solid lines showing the average values. In cases of channelization, the concentrations of each individual fracture geometry are also plotted. The insets in (c) plot the thickness of the altered layer in RF2 at hour 20 at a flow rate of 100 μL/min, and at hours 200 and 1000 at a flow rate of 10 μL/min, the inset in (d) plots the thickness of the altered layer in RF4 at hour 1000 at a flow rate of 10 μL/min.

The evolution of the hydraulic aperture does not necessarily follow that of the mechanical aperture (i.e., average fracture aperture) proportionally, as demonstrated by the ratio between the hydraulic and mechanical apertures (Figure 4(a)). In cases where the dissolution is localized at the inlet, the ratio decreases. This is because the downstream apertures are not enlarged and continue to constrain the flow, and the increase in apertures at the inlet does not translate into an increase in the hydraulic aperture. In cases of fracture channelization, an increase in the aperture ratio is observed after the breakthrough of the channel. The ratio can grow larger than unity, following the continuous development of the channel. As pointed out in previous studies, this disproportionally fast increase in the hydraulic aperture in comparison to that of the mechanical aperture is a characteristic feature of flow channeling.(40, 45) With uniform dissolution, the ratio between the hydraulic and mechanical aperture is close to unity. This proportional increase in hydraulic aperture with respect to mechanical aperture in uniformly dissolving fractures, however, may be suppressed or even inverted in the presence of confining stress.(12, 18, 28)
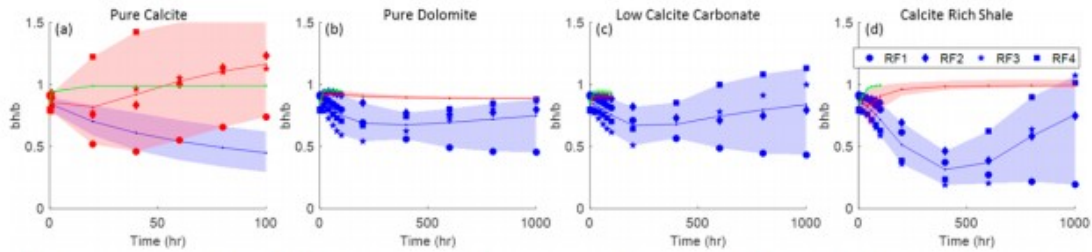
Figure 4. Evolution of the ratio between hydraulic aperture and average mechanical aperture at 10 (blue), 100 (red), and 1000 (green) $\mu L/min$ for the mineral composition of (a) pure calcite, (b) pure dolomite, (c) low calcite carbonate (i.e., the Duperow dolomite), and (d) calcite-rich shale (i.e., the Niobrara shale). The shaded areas illustrate the variations among different initial fracture geometries with the thin solid lines showing the average values. In cases of channelization, the results of each individual fracture are also plotted.

For the dolomite-only simulations (Figure 5), channelization is observed at a slower flow rate of 10 µL/min and at a later time step. Dissolution patterns are uniform at the two higher flow rates. After 1000 h of reactive flow at 10 µL/min, the opening of the dolomite fracture shows a smaller magnitude and more diffuse pattern than that of the calcite fractures at hour 100 at 100 µL/min, i.e., after the same number of pore volumes of fluid flow. This shift in the dissolution regime is attributed to the fact that the dissolution rate of dolomite is ~1 order of magnitude lower than that of calcite (Table 3).
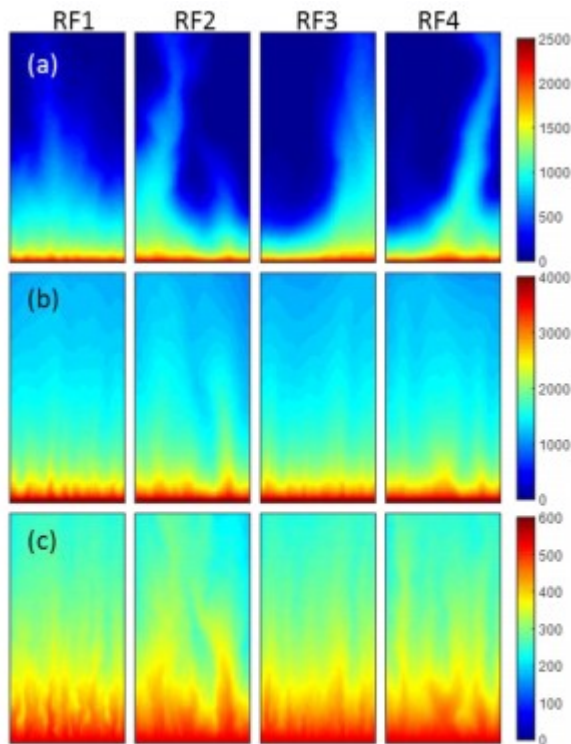
Figure 5. Simulated aperture change [μm] for the pure dolomite case after 1000 h of reactive flow at a rate of (a) 10 and (b) 100 $\mu L/min$ and (c) after 100 h of reaction at 1000 $\mu L/min$. Each column corresponds to an initial fracture geometry. From left to right: RF1–RF4.

Overall, for each dissolution regime, the evolution trajectory of the effluent chemistry and fracture hydraulic aperture are similar to those of the pure calcite case. The effluent Ca and Mg concentrations track each other (Figure

3(b) and (e)) because the dissolution is congruent. Both concentrations decrease over time at 10 μL/min as a result of increasingly focused flow and the decrease of effective surface area. The ratio between hydraulic and mechanical aperture decreases initially before the channel breakthrough, and increases after the channel is established (Figure 4(b)). At the two higher flow rates, the aperture ratio is maintained at about one through the entire course of the simulations. Unlike the pure calcite simulations, no temporal change is observed at the high flow rates because fracture volume increase and hence residence time change is limited. The effluent concentrations at a higher flow rate are lower than those at the slower flow rate due to shortened residence time and the transport limitation in the fracture plane on local reactions (Figure 3(b and e)).

3.1.2 The Role of Initial Fracture Geometry

The impacts of initial fracture geometry are secondary to those of the flow rates. Across the fracture geometries, the fracture evolution with respect to flow rate shows consistency. However, for a given dissolution regime, there are variations among different geometries. The variations are most evident when there is fracture channelization. Because local heterogeneity in fracture geometry is a major source of the perturbations that lead to fracture channelization, variations in the initial fracture aperture fields largely affect the initialization and development of channels.

In general, in random fields with less roughness and a shorter spatial correlation length (e.g., RF1), the channels are less developed after the same reaction time (Figures 2(b) and 5(a)). Accordingly, the decrease in the effluent cation concentration and thus overall dissolution rate (Figure 3(a, b, and e)) and the increase in the hydraulic–mechanical aperture ratio (Figure 4(a and b)) are observed at a later time step. For example, for the mineral composition of pure calcite, a flow channel is well established at 100 μL/min with an aperture ratio larger than 1 by hour 100 for all initial fracture geometries except RF1 (Figure 4(a)).

3.2 Heterogeneous Mineral Composition

Figure 6 plots the calcite aperture, which measures the distance between the calcite fronts in the two fracture halves in comparison with the flow aperture for the low calcite carbonate mineral composition, i.e., the Duperow dolomite. The former is of interest because the fast-reacting calcite plays an important role in controlling the progress of geochemical reactions affecting fluid in the fracture.
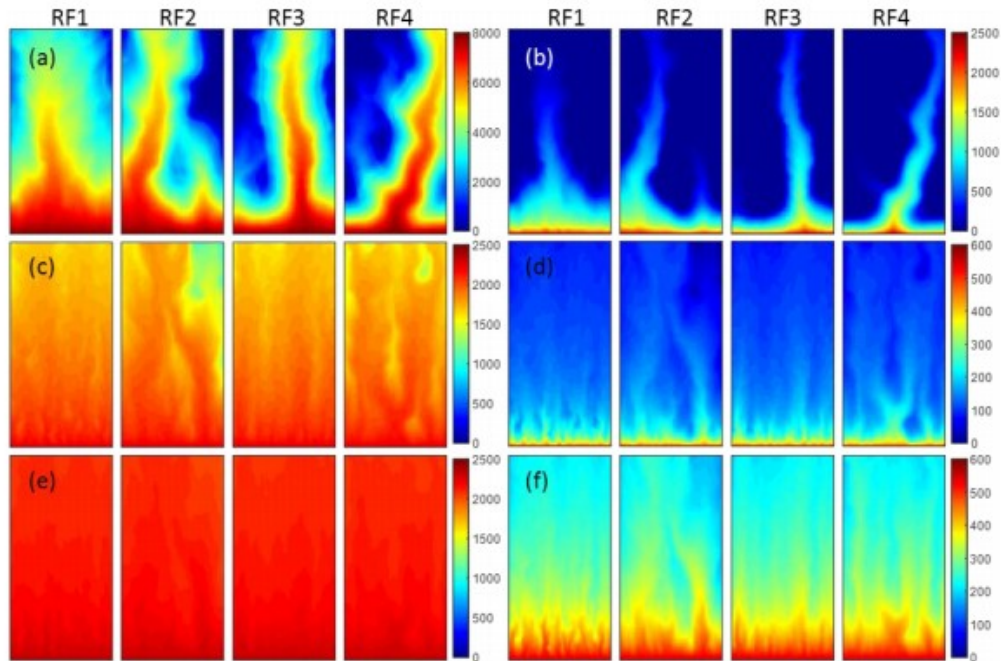
Figure 6. Simulated changes in calcite aperture (a, c, and e) and fracture aperture (b, d, and f) [μm] for the mineral composition of low calcite carbonate (i.e., the Duperow dolomite) after 1000 h of reactive flow at 10 μL/min (top panel) and after 100 h of reaction at 100 (middle panel) and 1000 (bottom) μL/min. In each subplot, each column corresponds to an initial fracture geometry. From left to right: RF1–RF4.

For this mineral composition, the flow aperture is controlled by dolomite dissolution. Similar to the dolomite-only cases, the fracture apertures increase uniformly at the flow rates of 100 and 1000 μL/min. At the flow rate of 10 μL/min, signs of channel development can be observed in the fractures at early time steps, and the channels become well-established at hour 1000. The spatial patterns of calcite apertures do not show similarity to those from the calcite-only simulations at the corresponding flow rate (Figure 2) and instead follow the spatial patterns of dolomite apertures, which control the fluid flow in the fractures. The spatial coverage of the altered layer also shows distinct patterns at different flow rates. The presence of the calcite, however, causes some deviations from the dolomite-only case. The magnitude of aperture increase is smaller, and the channels are narrower.

In this two-mineral simulation, the effluent concentrations of Mg and Ca show different temporal evolution trajectories (Figure 3(c and f)). The effluent Mg concentration is solely attributable to dolomite dissolution, whereas the effluent Ca concentration is a result of the dissolution of both calcite and dolomite but is dominated by calcite dissolution because of its more rapid dissolution rate. The decrease in Ca concentration is caused by the development of the altered layer and the resulting diffusion limitation. The altered layer diffusion limitation is the dominant factor at the higher flow rates for which the altered layer is more developed (Figure 3(c)). When channels develop (at 10 μL/min), even though the altered layer only covers a part of the fracture, the large thickness still results in considerable diffusion limitation on calcite dissolution (Figure 3(c)). In addition, the focusing of the fluid flow into the channel also contributes to the decrease in overall calcite

dissolution. This inference is supported by the observation that Ca concentration decreases more substantially in the fracture with stronger channelization. As a result of the reduced calcite dissolution over time, a lower pH is sustained in the fracture to promote the dissolution rate of dolomite. This pH effect offsets the decrease in dolomite dissolution due to flow channeling at 10 μL/min, resulting in a continuous increase in Mg concentration.

The hydraulic aperture increases as a result of the dissolution of dolomite at a rate that is similar to the mechanical aperture at flow rates of 100 and 1000 μL/min. Channelization at 10 μL/min causes a more rapid increase in the hydraulic aperture, leading to an increase in the hydraulic–mechanical aperture ratio after ~200 h except for RF1 (Figure 4(c)). The increase in the aperture ratio is more notable than the dolomite-only case because of the more focused channel development in this case.

Figure 7 plots the calcite and flow apertures from the simulations that use the Niobrara mineral composition, i.e., a calcite-rich shale. Results from simulations that use initial fracture aperture fields other than RF4 are not plotted because they show similar patterns. Although calcite apertures at different flow rates begin with spatial patterns that are similar to the calcite-only case with the same initial fracture aperture field (Figure 7(a, d, and f) at hour 100), channels form at 10 μL/min instead of 100 μL/min and at later times (e.g., hour 1000, Figure 7(b)). Given the slow reaction kinetics of minerals other than calcite, dissolution of minerals remaining in the altered layer do not cause an observable change in fracture apertures. Rather, the fracture apertures increase as a result of the detachment or erosion of the altered layer. This erosion process is triggered by the dissolution of the cementing material, i.e., calcite, and thus, fracture apertures closely track calcite apertures (Figure 7 (c and f)). Because sufficient calcite has to be removed for disaggregation and detachment of the altered layer to happen, calcite dissolution does not lead to an immediate change in the fracture aperture and flow field. The delay in the feedback between the flow and the reaction causes the shift in the dissolution regime.
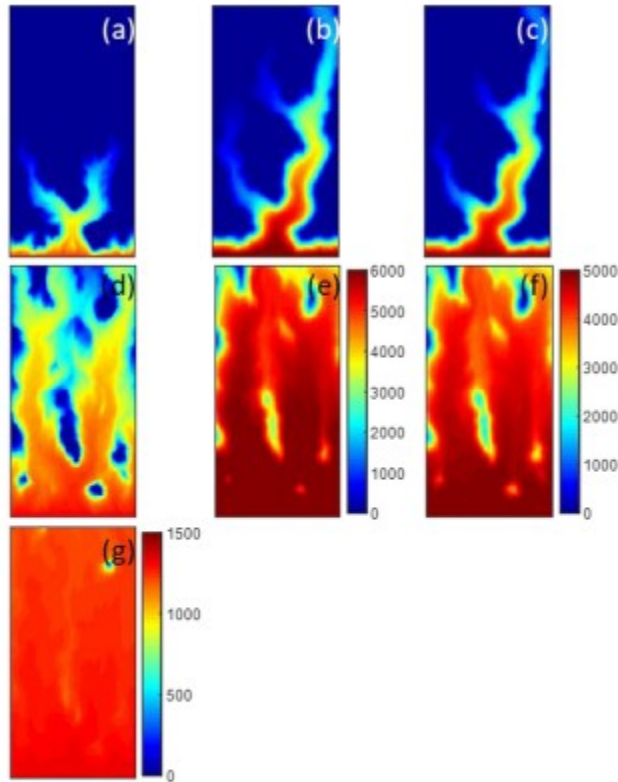
Figure 7. Simulated changes in calcite aperture (a, b, d, e, and g) and fracture aperture (c and f) [μm] for the mineral composition of calcite-rich shale (i.e., the Niobrara shale) and RF4 at 10 (top panel), 100 (middle panel), and 1000 (bottom) $\mu L/min$. The left column shows results after 100 h, and the rest are after 1000 h of reactive flow. The same color bar is used in each column.

Calcite dissolution, as indicated by the effluent Ca concentrations, decreases as a result of the diffusion limitation of the altered layer at the higher flow rates (Figure 3(d)). Diffusion limitation is less important at the lower flow rate (10 µL/min) because of the highly localized altered layer development. The decrease is instead primarily associated with flow channeling. The channelization also corresponds to an increase in the hydraulic–mechanical aperture ratio (Figure 4(d)). A minor increase in the aperture ratio is also observed at early times at 100 µL/min because the fracture opening is not yet uniform, and the shape of the channels observed in the calcite-only case can still be identified (Figure 7(f)).

3.3 Time Scale Analysis

The results of the numerical experiments demonstrate distinct behavior of fracture evolution for different mineral compositions. The interplay between flow and reactions that ultimately controls fracture alteration can be summarized by the conceptual models (Figure 8) for each category of mineral composition.
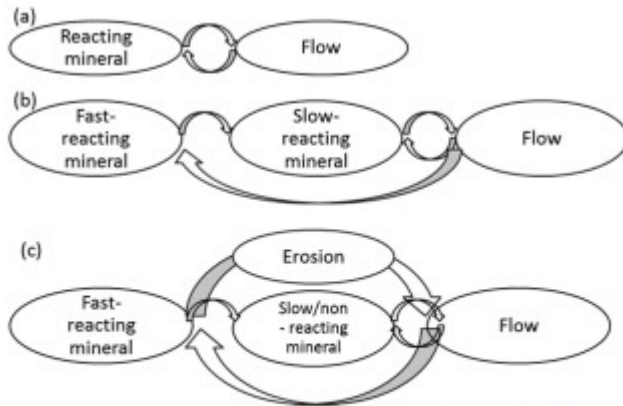
Figure 8. Conceptual models of the reaction-flow feedback loops for (a) a single mineral, (b) minerals of differing reactivity, and (c) minerals of differing reactivity and with erosion.

With a single mineral, the feedback between reaction and flow constitutes a complete and simple loop. In the presence of multiple minerals, the feedback loops become more complicated. In multimineral systems where the intact rock matrix has a low percentage of a fast reacting mineral, i.e. the altered layer has a low porosity and no detachment, fracture evolution is controlled by the feedback between the reaction of the slow-reacting mineral and the flow. Whether there is fracture channelization and what the breakthrough time is are controlled by the slow-reacting mineral. However, an additional indirect feedback may exist, because the reaction rate of the slow-reacting mineral may also be affected by the fast-reacting mineral, which is in turn influenced by the flow field in the fracture.

In multimineral systems where the fast-reacting mineral is the cementing material and accounts for a large fraction such that it supports the structure of the intact rock matrix, the dominant feedback loop is the one between flow and the fast-reacting mineral. Regardless of the presence of effectively nonreactive minerals in the remaining altered layer, fracture aperture change and thus the continuous feedback between reaction and flow is enabled by the erosion of the altered layer. There is, however, a delay in the feedback, resulting in shifts in the flow regime that eventually leads to fracture channelization.

In single mineral systems, the dimensionless Damköhler number has typically been used to measure the interplay between flow and reactions. It is defined as the ratio between the time scale of advection (τ_{ad}) and reaction (τ_{rxn}) and has proven to be useful for investigating the evolution of fractures of different lengths and at different flow rates. Here, on the basis of the conceptual models, we propose a multireaction Damköhler number (mDa) to extend the use of the traditional Damköhler number into multimineral systems in which minerals of differing reactivity are mixed.

In general, the time scale of advection (τ_{ad}) is defined as the ratio between the fracture volume V_{frac} and the volumetric flow rate

$$Q. \quad \tau_{ad} = \frac{V_{frac}}{Q} \quad (9)$$

The time scale of the reaction in fractures (τ_{rxn}) is calculated from the characteristic length (i.e., the average fracture aperture, $\bar{b}$) and a rate constant (k_b). The rate constant measures the rate of fracture aperture change due to mineral reactions and has units of m/s.

$$\tau_{rxn} = \frac{\bar{b}}{k_b} \quad (10)$$

k_b is related to the kinetic coefficient (k_{rxn}, [mol m^{-2} s^{-1}]) under far-from-equilibrium conditions as

$$\blacksquare \quad (11)$$

where A_{rxn} is the reactive surface area [m^2], V_{mol} is the molar volume of the mineral [m^3 mineral/mol], f_r represents the volume fraction of the mineral in the rock matrix [$\frac{m^3 \text{ mineral}}{m^3 \text{ porous media}}$], and A is the geometric surface area. As shown in Table 3, the kinetic coefficient may depend on different reaction pathways (eq 12),

$$k_{rxn} = \sum (k_i a_i) \quad (12)$$

where k_i is the kinetic coefficient of the respective pathway, and a_i is the activity of the corresponding catalytic or inhibitory species i.

Assuming that the reactive surface area is simply the geometric surface area of the two fracture halves, eq 11 can be simplified to

$$\blacksquare \quad (13)$$

In multimineral systems, the rate of aperture change can be calculated for each mineral ($k_{b,m}$) based on its respective kinetic coefficient, molar volume, and volume fraction.

$$\blacksquare \quad (14)$$

Without erosion, such as in the case of the low calcite carbonate, the actual fracture aperture is controlled by the mineral front that retreats the slowest. Then, the rate of fracture aperture change is given by the minimum of the rates of aperture change for all minerals present.

$$k_b = \min\{k_{b,m_1}, \ldots, k_{b,m_c}\} \quad (15)$$

For cases where there is erosion, the rate of fracture aperture change is controlled primarily by the rate of aperture change of the fast reacting

mineral ($m*$). We can then use the reaction rate of the fast-reacting mineral as a surrogate for the rate of fracture aperture change.

$$k_b = k_{b,m*} \quad (16)$$

However, because the erosion occurs when the altered layer exceeds a critical thickness, the diffusion limitation from the altered layer is substantial, and the effective reaction rate should be used.

$$(17)$$

$$(18)$$

The diffusion-controlled rate is given by the effective diffusion coefficient and the critical thickness of the altered layer. The equilibrium concentration, molar volume, and mineral volume fraction are used to convert the unit from m/s for aqueous species to m/s for the solid fracture surface.

For the erosion case, another time scale (τ_{ero}), the time needed for the thickness of the altered layer to reach the critical threshold, should be included in the multireaction Damköhler number calculation so as to account for the observation that the erosion does not occur until a certain amount of cementing material is dissolved.

$$\tau_{ero} = \frac{L_c}{k_{rxn,m*}} \quad (19)$$

$$mDa = \frac{\tau_{ad}}{\tau_{rxn} + \tau_{ero}} \quad (20)$$

On the basis of the proposed extended framework, the multireaction Damköhler number is calculated for all simulations. For the calcite-only case, the multireaction Damköhler number is the same as the traditional Damköhler number. It is ~6.4 × 10^{-3} at 100 µL/min when evident fracture channelization is observed. The Damköhler number is larger at the lower flow rate under which fracture opening is localized at the inlet, whereas the value is smaller at the higher flow rate where fracture opening is uniform.

$$(21)$$

$$(22)$$

For the dolomite-only and low calcite carbonate cases (eq 21), fracture channelization is observed at the flow rate of 10 µL/min. The multireaction Damköhler number values are 6.7 × 10^{-3} and 6.1 × 10^{-3}, respectively, and are consistent with the calcite-only calculation. For the calcite-rich shale case for which fracture opening depends on the detachment of the altered layer

(eq 22), the multireaction Damköhler number values at 10 μL/min ranges from 9.5×10^{-3} to 1.6×10^{-2} for the four fracture geometries with an average of 1.3×10^{-3}. The values are only higher than the multireaction Damköhler number values in the channelization regime reported for the other mineral compositions by a factor of ~2. Even though calcite dissolution is the ultimate driving force for fracture opening, the calculated multireaction Damköhler number values are smaller than those of the calcite-only case at the same flow rate by a factor of ~5. This is consistent with the observation that channelization is observed at the lower flow rate for the Niobrara mineral composition and illustrates that the proposed framework successfully captures the underlying processes of fracture alteration in multimineral systems.

It should be noted that there are some limitations of using this framework of the Damköhler number. For example, it does not account for mineral spatial heterogeneity. However, it provides a useful framework for the analysis of fracture evolution in well-mixed multimineral systems. For example, the multireaction Damköhler number can be used to predict the change in fracture dissolution patterns caused by the change in calcite content, which is also consistent with results from reactive transport simulations as demonstrated below.

Figure 9 shows the changes in fracture aperture fields after 1000 h of reactive flow at the flow rate of 10 μL/min for low calcite carbonates that have a calcite content of 5, 20, and 30%, respectively. As the calcite content increases, there is a shift from channelization to compact dissolution. With 5% calcite, the channel has penetrated the fracture, and the ratio between hydraulic and mechanical aperture has started to increase by hour 1000. In contrast, with 30% of calcite, the channel is limited to the inlet, and the aperture ratio is still decreasing. Additionally, as calcite content increases, the decrease in Ca concentration and the increase in Mg concentration are less significant after the same amount of fluid flow because it takes longer for the channel to break through. This observation is consistent across different fracture geometries.
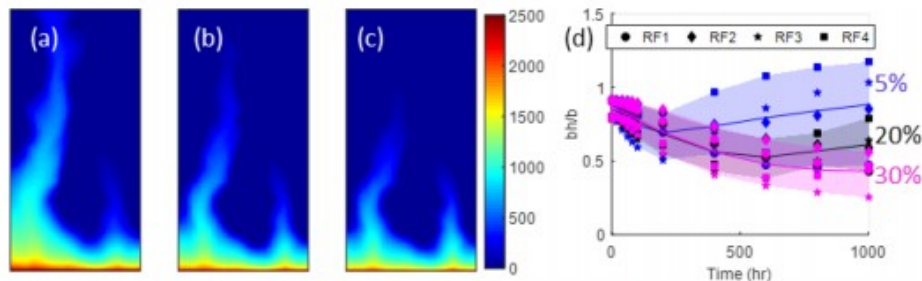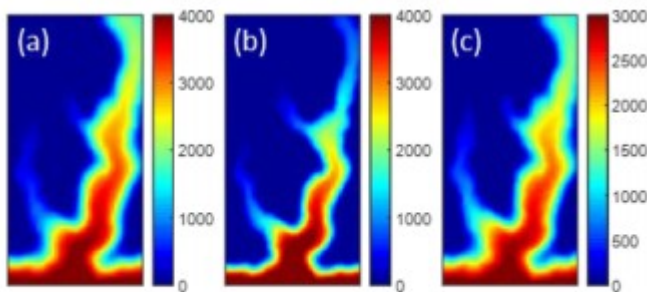

Figure 9. Simulated changes in fracture aperture [μm] for the low calcite carbonates with (a) 5, (b) 20, and (c) 30% calcite using RF2 after 1000 h of reactive flow at 10 μL/min. (d) Temporal evolution of the ratio between hydraulic and mechanical aperture.

Similar conclusions can be drawn from the proposed multireaction Damköhler number framework (eq 21). With higher calcite content, i.e., a smaller volume fraction of dolomite, the multireaction Damköhler number

increases corresponding to a shift from channelization to a compact dissolution regime.

Similarly, the proposed framework allows analysis of calcite content variations and the impact on the evolution of calcite-rich shale fractures. For RF4 (Figure 10), the fracture aperture change is more focused at the inlet as calcite content increases from 35 to 60%, corresponding to a delay in the increase of the hydraulic–geometry aperture ratio. This appears to contradict the observation that the multireaction Damköhler number decreases as $f_{r,cal}$ increases. However, in this case, the effective diffusion coefficient in the altered layer, which also affects the reaction rate, increases as the calcite content increases. This would lead to an increase in the multireaction Damköhler number and therefore offsets the effect of $f_{r,cal}$.

Figure 10. Simulated changes in fracture aperture [μm] for the calcite-rich shale simulations with (a, c) 35 and (b) 60% calcite using RF4 after 1000 h of reactive flow at 10 $\mu L/min$. (c) A larger critical thickness is used for the calculation of the altered layer erosion.

In the two simulations discussed above, the same critical thickness reported for a Niobrara (with ~50% calcite) experiment was assumed. However, it is likely that, with a higher calcite content, the critical thickness is lower given the more weakened structure of the altered layer. Assuming the critical thickness is inversely proportional to calcite content and thus using a larger critical thickness for the lower calcite content (35%) simulation results in slightly enhanced development of the left branch of the channel. This is consistent with a decrease in the multireaction Damköhler number as L_c increases and a transition toward the uniform dissolution regime. The critical thickness (L_c) is dependent on mineral composition and texture. Although future studies are needed to provide more quantitative understanding of L_c as a function of mineralogy and rock texture, the multireaction Damköhler number can be used to provide insights regarding fracture alteration for a range of reasonable L_c values.

These simulations demonstrate that many factors come into play in controlling the spatial patterns of fracture dissolution in multimineral systems, and the multireaction Damköhler number proposed can be useful in examining the compound effects.

4 Implications

In our study, a reduced dimension reactive transport model validated previously was used to investigate the impacts of mineral composition, flow rate, and geometric heterogeneity on fracture alteration. The results of the numerical experiments were used to develop a multireaction Damköhler number that extends the use of the traditional Damköhler number from single mineral systems to multimineral systems. The multireaction Damköhler number provides a useful tool for the prediction of fracture dissolution patterns in systems where minerals of differing reactivity coexist, which can be found in Earth's critical zone and deep geological systems such as granite and various sedimentary rocks. Here, as an example, we discuss some important insights regarding caprock integrity and the leakage risk of geologic carbon storage based on our findings.

The risk of brine leakage through pre-existing fractures in caprocks will depend on the dissolution regimes of fractures after being exposed to CO_2-acidified brine. In the compact dissolution regime, the risk of leakage is low, whereas the leakage risk is high with channelization because continuous flow channels are maintained. In the uniform dissolution regime, the risk largely depends on the stress conditions. The leakage risk may be low under confining stress as fractures in the uniform dissolution regime are likely to close in response. Otherwise, the leakage risk can be high.

The traditional Damköhler number provides a useful framework for analyzing fracture dissolution regimes at different fracture lengths and flow rates in single mineral systems. Using the Damköhler number as a guide, insights derived from a limited number of experimental studies can be used to predict the dissolution regimes and caprock leakage risk for a range of pressure conditions and fracture geometries for the same mineral. Our study extends this framework to multimineral systems, such that a similar workflow can be applied to evaluate leakage risks in caprocks with various mineral compositions. The value of the multireaction Damköhler number for different dissolution regimes can be determined from laboratory experiments. Then, the flow rates that correspond to different dissolution regimes can be estimated for a fracture with a given length and mineral composition. Leakage risk can then be assessed for a range of flow conditions that are dictated by the pressure gradient and the fracture hydraulic apertures in the field (Figure 11).
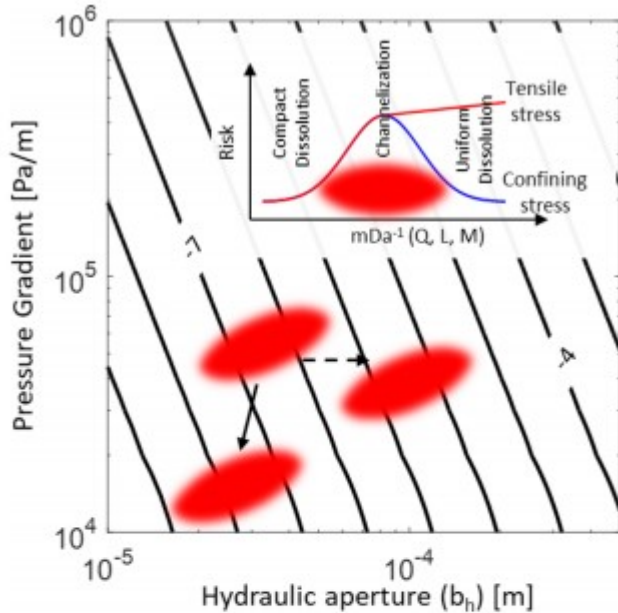
Figure 11. Conceptual and simplified analysis of leakage risk based on the proposed framework. Flow rate (Q) [log m³ s⁻¹] contours are plotted with respect to fracture hydraulic aperture and pressure gradient. (inset) Conceptual figure showing the dissolution regime at different values of Damköhler number (mDa) and the corresponding leakage risk under different stress conditions. Please note that the multireaction Damköhler number is a function of flow rate (Q), fracture length (L), and mineral composition (M). The red ellipse encompasses the region with flow conditions corresponding to high leakage risks for a given case. The solid arrow illustrates the shift of the high risk flow regime from a calcite fracture to fractures in rocks with more complex mineral composition, and the dashed arrow exemplifies the shift of the high risk flow regime as fracture length increases.

For example, as illustrated in Figure 11, with elevated pressure and thus higher flow rates, fractures in formations composed of calcite are more likely to be in the regime of channelization compared to fractures in the rock matrix of a more complex mineral composition, which are likely to be in the uniform dissolution regime. It is also indicated that, with all conditions held the same, as the fracture length increases, calcite fractures may switch from channelization to compact dissolution and therefore leads to lower risks. In contrast, fractures in low calcite carbonates and calcite-rich shales may switch from uniform dissolution to channelization and therefore maintain a high risk.

The authors declare no competing financial interest.

References

(1) Aydin, A. Fractures, faults, and hydrocarbon entrapment, migration and flow. Mar. Pet. Geol. 2000, 17 (7), 797−814. (2) Palmer, A. N. ORIGIN AND MORPHOLOGY OF LIMESTONE CAVES. Geol. Soc. Am. Bull. 1991, 103 (1), 1−21. (3) DePaolo, D. J.; Orr, F. M., Jr. Geoscience research for our energy future. Phys. Today 2008, 61 (8), 46−51. (4) Lin, H. Earth's Critical Zone and hydropedology: concepts, characteristics, and advances. Hydrol. Earth Syst. Sci. 2010, 14 (1), 25− 45. (5) Anderson, S. P.; Dietrich, W. E.; Montgomery, D. R.; Torres, R.; Conrad, M. E.; Loague, K. Subsurface flow paths in a steep, unchanneled catchment. Water Resour. Res. 1997, 33 (12), 2637−2653. (6) Etiope, G.; Martinelli, G. Migration of carrier and trace gases in the geosphere: an overview. Phys. Earth Planet. Inter. 2002, 129 (3−4), 185−204. (7) McCarthy, J. F.; McKay, L. D. Colloid transport in the subsurface: Past, present, and future challenges. Vadose Zone J. 2004, 3 (2), 326−337. (8) St. Clair, J.; Moon, S.; Holbrook, W. S.; Perron, J. T.; Riebe, C. S.; Martel, S. J.; Carr, B.; Harman, C.; Singha, K.; Richter, D. D. Geophysical imaging reveals topographic stress control of bedrock weathering. Science 2015, 350 (6260), 534−538. (9) Tian, H. L.; Pan, F.; Xu, T. F.; McPherson, B. J.; Yue, G. F.; Mandalaparty, P. Impacts of hydrological heterogeneities on caprock mineral alteration and containment of CO2 in geological storage sites. Int. J. Greenhouse Gas Control 2014, 24, 30−42. (10) Neuman, S. P. Trends, prospects and challenges in quantifying flow and transport through fractured rocks. Hydrogeol. J. 2005, 13 (1), 124−147. (11) Detwiler, R.; Glass, R.; Bourcier, W. Experimental observations of fracture dissolution: The role of Peclet number on evolving aperture variability. Geophys. Res. Lett. 2003, 30 (12), 1648−1651. (12) Detwiler, R. Experimental observations of deformation caused by mineral dissolution in variable-aperture fractures. J. Geophys. Res. 2008, 113 (B8), 1. (13) Elkhoury, J. E.; Ameli, P.; Detwiler, R. L. Dissolution and deformation in fractured carbonates caused by flow of CO2-rich brine under reservoir conditions. Int. J. Greenhouse Gas Control 2013, 16, Supplement 1 (0), S203−S215. (14) Garcia-Rios, M.; Luquot, L.; Soler, J. M.; Cama, J. Influence of the flow rate on dissolution and precipitation features during percolation of CO2-rich sulfate solutions through fractured limestone samples. Chem. Geol. 2015, 414, 95−108. (15) Szymczak, P.; Ladd, A. J. C. Wormhole formation in dissolving fractures. J. Geophys. Res. 2009, 114, B06203. (16) Steefel, C. I.; Lasaga, A. C. EVOLUTION OF DISSOLUTION PATTERNS - PERMEABILITY CHANGE DUE TO COUPLED FLOW AND REACTION. ACS Symp. Ser. 1990, 416, 212−225. (17) Ortoleva, P.; Merino, E.; Moore, C.; Chadam, J. GEOCHEMICAL SELF-ORGANIZATION 0.1. REACTION-TRANSPORT FEEDBACKS AND MODELING APPROACH. Am. J. Sci. 1987, 287 (10), 979−1007. (18) Ameli, P.; Elkhoury, J.; Morris, J.; Detwiler, R. Fracture Permeability Alteration due to Chemical and Mechanical Processes: A Coupled High-Resolution Model. Rock Mechanics and Rock Engineering 2014, 47 (5), 1563−1573. (19) Xiao, T.; Kweon, H.; McPherson, B.; Deo, M. Wormhole Generations in Indiana Limestone with CO2 Intrusion: Numerical Simulations Based on Core Flooding Experiments. Energy Fuels 2017, 31 (11), 12487−12499. (20) Molins, S.; Trebotich, D.; Miller, G. H.; Steefel, C. I.

Mineralogical and transport controls on the evolution of porous media texture using direct numerical simulation. Water Resour. Res. 2017, 53 (5), 3645−3661. (21) Wen, H.; Li, L.; Crandall, D.; Hakala, A. Where Lower Calcite Abundance Creates More Alteration: Enhanced Rock Matrix Diffusivity Induced by Preferential Dissolution. Energy Fuels 2016, 30 (5), 4197−4208. (22) Gouze, P.; Noiriel, C.; Bruderer, C.; Loggia, D.; Leprovost, R. Xray tomography characterization of fracture surfaces during dissolution. Geophys. Res. Lett. 2003, 30 (5), 1267. (23) Noiriel, C.; Made, B.; Gouze, P. Impact of coating development on the hydraulic and transport properties in argillaceous limestone fracture. Water Resour. Res. 2007, 43 (9), W09406. (24) Andreani, M.; Gouze, P.; Luquot, L.; Jouanna, P. Changes in seal capacity of fractured claystone caprocks induced by dissolved and gaseous CO2 seepage. Geophys. Res. Lett. 2008, 35 (14), L14404. (25) Noiriel, C.; Gouze, P.; Made, B. 3D analysis of geometry and flow changes in a limestone fracture during dissolution. J. Hydrol. 2013, 486, 211−223. (26) Davila, G.; Luquot, L.; Soler, J. M.; Cama, J. Interaction between a fractured marl caprock and CO2-rich sulfate solution under supercritical CO2 conditions. Int. J. Greenhouse Gas Control 2016, 48, 105−119. (27) Garcia-Rios, M.; Luquot, L.; Soler, J. M.; Cama, J. The role of mineral heterogeneity on the hydrogeochemical response of two fractured reservoir rocks in contact with dissolved CO2. Appl. Geochem. 2017, 84, 202−217. (28) Elkhoury, J. E.; Detwiler, R. L.; Ameli, P. Can a fractured caprock self-heal? Earth Planet. Sci. Lett. 2015, 417, 99−106. (29) Ellis, B. R.; Peters, C. A.; Fitts, J.; Bromhal, G.; McIntyre, D.; Warzinski, R.; Rosenbaum, E. Deterioration of a fractured carbonate caprock exposed to CO2-acidified brine flow. Greenhouse Gases: Sci. Technol. 2011, 1 (3), 248−260. (30) Ellis, B. R.; Fitts, J. P.; Bromhal, G. S.; McIntyre, D. L.; Tappero, R.; Peters, C. A. Dissolution-Driven Permeability Reduction of a Fractured Carbonate Caprock. Environ. Eng. Sci. 2013, 30 (4), 187− 193. (31) Noiriel, C.; Gouze, P.; Made, B. Time-resolved 3D character-́ isation of flow and dissolution patterns in a single rough-walled fracture. In Groundwater in Fractured Rocks; Jirí Krasny ́, J. M. S., Ed.;́ Taylor & Francis, 2007; pp 629−642. (32) Navarre-Sitchler, A.; Steefel, C. I.; Sak, P. B.; Brantley, S. L. A reactive-transport model for weathering rind formation on basalt. Geochim. Cosmochim. Acta 2011, 75 (23), 7644−7667. (33) Chen, L.; Kang, Q.; Carey, B.; Tao, W.-Q. Pore-scale study of diffusion-reaction processes involving dissolution and precipitation using the lattice Boltzmann method. Int. J. Heat Mass Transfer 2014, 75, 483−496. (34) Deng, H.; Voltolini, M.; Molins, S.; Steefel, C.; DePaolo, D.; Ajo-Franklin, J.; Yang, L. Alteration and Erosion of Rock Matrix Bordering a Carbonate-Rich Shale Fracture. Environ. Sci. Technol. 2017, 51 (15), 8861−8868. (35) Deng, H.; Molins, S.; Steefel, C.; DePaolo, D.; Voltolini, M.; Yang, L.; Ajo-Franklin, J. A 2.5D Reactive Transport Model for Fracture Alteration Simulation. Environ. Sci. Technol. 2016, 50 (14), 7564−7571. (36) Hao, Y.; Smith, M.; Sholokhova, Y.; Carroll, S. CO2-induced dissolution of low permeability carbonates. Part II: Numerical modeling of experiments. Adv. Water Resour. 2013, 62, 388−408. (37) Steefel, C. I.; Appelo, C. A. J.; Arora, B.; Jacques, D.; Kalbacher, T.;

Kolditz, O.; Lagneau, V.; Lichtner, P. C.; Mayer, K. U.; Meeussen, J. C. L.; Molins, S.; Moulton, D.; Shao, H.; Simunek, J.; Spycher, N.; Yabusaki, S. B.; Yeh, G. T. Reactive transport codes for subsurface environmental simulation. Computational Geosciences 2015, 19 (3), 445−478. (38) Snow, D. T. ANISOTROPIC PERMEABILITY OF FRACTURED MEDIA. Water Resour. Res. 1969, 5 (6), 1273−1289. (39) Chen, L.; Kang, Q.; Viswanathan, H. S.; Tao, W.-Q. Pore-scale study of dissolution-induced changes in hydrologic properties of rocks with binary minerals. Water Resour. Res. 2014, 50 (12), 9343−9365. (40) Deng, H.; Fitts, J. P.; Crandall, D.; McIntyre, D.; Peters, C. A. Alterations of Fractures in Carbonate Rocks by CO2-Acidified Brines. Environ. Sci. Technol. 2015, 49 (16), 10226−10234. (41) Ajo-Franklin, J. V.; Molins, S.; Yang, L. Coupled Processes in a Fractured Reactive System: A Dolomite Dissolution Study with Relevance to GCS Caprock Integrity. In Caprock Integrity in Geological Storage: Hydrogeochemical and Hydrogeomechanical Processes and their Impact on Storage Security; Wiley Publishing, 2017. (42) Bourg, I. C. Sealing Shales versus Brittle Shales: A Sharp Threshold in the Material Properties and Energy Technology Uses of Fine-Grained Sedimentary Rocks. Environ. Sci. Technol. Lett. 2015, 2 (10), 255−259. (43) Palandri, J. L. K., Yousif, K. A compilation of rate parameters of water-mineral interaction kinetics for application to geochemical modeling; U.S. Dept. of the Interior, U.S. Geological Survey: Menlo Park, Calif, 2004. (44) Marty, N. C. M.; Claret, F.; Lassin, A.; Tremosa, J.; Blanc, P.; Made, B.; Giffaut, E.; Cochepin, B.; Tournassat, C. A database of dissolution and precipitation rates for clay-rocks minerals. Appl. Geochem. 2015, 55, 108−118. (45) Hanna, R. B.; Rajaram, H. Influence of aperture variability on dissolutional growth of fissures in karst formations. Water Resour. Res. 1998, 34 (11), 2843−2853.